

Measurement of Non-Random Event-by-Event Fluctuations of Average Transverse Momentum in $\sqrt{s_{NN}} = 200$ GeV Au+Au and p+p Collisions

S.S. Adler,⁵ S. Afanasiev,¹⁷ C. Aidala,⁵ N.N. Ajitanand,⁴³ Y. Akiba,^{20,38} J. Alexander,⁴³ R. Amirikas,¹² L. Aphecetche,⁴⁵ S.H. Aronson,⁵ R. Averbeck,⁴⁴ T.C. Awes,³⁵ R. Azmoun,⁴⁴ V. Babintsev,¹⁵ A. Baldisseri,¹⁰ K.N. Barish,⁶ P.D. Barnes,²⁷ B. Bassalleck,³³ S. Bathe,³⁰ S. Batsouli,⁹ V. Baublis,³⁷ A. Bazilevsky,^{39,15} S. Belikov,^{16,15} Y. Berdnikov,⁴⁰ S. Bhagavatula,¹⁶ J.G. Boissevain,²⁷ H. Borel,¹⁰ S. Borenstein,²⁵ M.L. Brooks,²⁷ D.S. Brown,³⁴ N. Bruner,³³ D. Bucher,³⁰ H. Buesching,³⁰ V. Bumazhnov,¹⁵ G. Bunce,^{5,39} J.M. Burward-Hoy,^{26,44} S. Butsyk,⁴⁴ X. Camard,⁴⁵ J.-S. Chai,¹⁸ P. Chand,⁴ W.C. Chang,² S. Chernichenko,¹⁵ C.Y. Chi,⁹ J. Chiba,²⁰ M. Chiu,⁹ I.J. Choi,⁵² J. Choi,¹⁹ R.K. Choudhury,⁴ T. Chujo,⁵ V. Cianciolo,³⁵ Y. Cobigo,¹⁰ B.A. Cole,⁹ P. Constantin,¹⁶ D.G. d'Enterria,⁴⁵ G. David,⁵ H. Delagrange,⁴⁵ A. Denisov,¹⁵ A. Deshpande,³⁹ E.J. Desmond,⁵ O. Dietzsch,⁴¹ O. Drapier,²⁵ A. Drees,⁴⁴ R. du Rietz,²⁹ A. Durum,¹⁵ D. Dutta,⁴ Y.V. Efremenko,³⁵ K. El Chenawi,⁴⁹ A. Enokizono,¹⁴ H. En'yo,^{38,39} S. Esumi,⁴⁸ L. Ewell,⁵ D.E. Fields,^{33,39} F. Fleuret,²⁵ S.L. Fokin,²³ B.D. Fox,³⁹ Z. Fraenkel,⁵¹ J.E. Frantz,⁹ A. Franz,⁵ A.D. Frawley,¹² S.-Y. Fung,⁶ S. Garpman,^{29,*} T.K. Ghosh,⁴⁹ A. Glenn,⁴⁶ G. Gogoberidze,⁴⁶ M. Gonin,²⁵ J. Gosset,¹⁰ Y. Goto,³⁹ R. Granier de Cassagnac,²⁵ N. Grau,¹⁶ S.V. Greene,⁴⁹ M. Grosse Perdekamp,³⁹ W. Guryan,⁵ H.-Å. Gustafsson,²⁹ T. Hachiya,¹⁴ J.S. Haggerty,⁵ H. Hamagaki,⁸ A.G. Hansen,²⁷ E.P. Hartouni,²⁶ M. Harvey,⁵ R. Hayano,⁸ X. He,¹³ M. Heffner,²⁶ T.K. Hemmick,⁴⁴ J.M. Heuser,⁴⁴ M. Hibino,⁵⁰ J.C. Hill,¹⁶ W. Holzmann,⁴³ K. Homma,¹⁴ B. Hong,²² A. Hoover,³⁴ T. Ichihara,^{38,39} V.V. Ikonnikov,²³ K. Imai,^{24,38} D. Eisenhower,¹ M. Ishihara,³⁸ M. Issah,⁴³ A. Isupov,¹⁷ B.V. Jacak,⁴⁴ W.Y. Jang,²² Y. Jeong,¹⁹ J. Jia,⁴⁴ O. Jinnouchi,³⁸ B.M. Johnson,⁵ S.C. Johnson,²⁶ K.S. Joo,³¹ D. Jouan,³⁶ S. Kametani,^{8,50} N. Kamihara,^{47,38} J.H. Kang,⁵² S.S. Kapoor,⁴ K. Katou,⁵⁰ S. Kelly,⁹ B. Khachaturov,⁵¹ A. Khanzadeev,³⁷ J. Kikuchi,⁵⁰ D.H. Kim,³¹ D.J. Kim,⁵² D.W. Kim,¹⁹ E. Kim,⁴² G.-B. Kim,²⁵ H.J. Kim,⁵² E. Kistenev,⁵ A. Kiyomichi,⁴⁸ K. Kiyoyama,³² C. Klein-Boesing,³⁰ H. Kobayashi,^{38,39} L. Kochenda,³⁷ V. Kochetkov,¹⁵ D. Koehler,³³ T. Kohama,¹⁴ M. Kopytine,⁴⁴ D. Kotchetkov,⁶ A. Kozlov,⁵¹ P.J. Kroon,⁵ C.H. Kuberg,^{1,27} K. Kurita,³⁹ Y. Kuroki,⁴⁸ M.J. Kweon,²² Y. Kwon,⁵² G.S. Kyle,³⁴ R. Lacey,⁴³ V. Ladygin,¹⁷ J.G. Lajoie,¹⁶ A. Lebedev,^{16,23} S. Leckey,⁴⁴ D.M. Lee,²⁷ S. Lee,¹⁹ M.J. Leitch,²⁷ X.H. Li,⁶ H. Lim,⁴² A. Litvinenko,¹⁷ M.X. Liu,²⁷ Y. Liu,³⁶ C.F. Maguire,⁴⁹ Y.I. Makdisi,⁵ A. Malakhov,¹⁷ V.I. Manko,²³ Y. Mao,^{7,38} G. Martinez,⁴⁵ M.D. Marx,⁴⁴ H. Masui,⁴⁸ F. Matathias,⁴⁴ T. Matsumoto,^{8,50} P.L. McGaughey,²⁷ E. Melnikov,¹⁵ F. Messer,⁴⁴ Y. Miake,⁴⁸ J. Milan,⁴³ T.E. Miller,⁴⁹ A. Milov,^{44,51} S. Mioduszewski,⁵ R.E. Mischke,²⁷ G.C. Mishra,¹³ J.T. Mitchell,⁵ A.K. Mohanty,⁴ D.P. Morrison,⁵ J.M. Moss,²⁷ F. Mühlbacher,⁴⁴ D. Mukhopadhyay,⁵¹ M. Muniruzzaman,⁶ J. Murata,^{38,39} S. Nagamiya,²⁰ J.L. Nagle,⁹ T. Nakamura,¹⁴ B.K. Nandi,⁶ M. Nara,⁴⁸ J. Newby,⁴⁶ P. Nilsson,²⁹ A.S. Nyanyi,²³ J. Nystrand,²⁹ E. O'Brien,⁵ C.A. Ogilvie,¹⁶ H. Ohnishi,^{5,38} I.D. Ojha,^{49,3} K. Okada,³⁸ M. Ono,⁴⁸ V. Onuchin,¹⁵ A. Oskarsson,²⁹ I. Otterlund,²⁹ K. Oyama,⁸ K. Ozawa,⁸ D. Pal,⁵¹ A.P.T. Palounek,²⁷ V.S. Pantuev,⁴⁴ V. Papavassiliou,³⁴ J. Park,⁴² A. Parmar,³³ S.F. Pate,³⁴ T. Peitzmann,³⁰ J.-C. Peng,²⁷ V. Peresedov,¹⁷ C. Pinkenburg,⁵ R.P. Pisani,⁵ F. Plasil,³⁵ M.L. Purschke,⁵ A.K. Purwar,⁴⁴ J. Rak,¹⁶ I. Ravinovich,⁵¹ K.F. Read,^{35,46} M. Reuter,⁴⁴ K. Reygers,³⁰ V. Riabov,^{37,40} Y. Riabov,³⁷ G. Roche,²⁸ A. Romana,²⁵ M. Rosati,¹⁶ P. Rosnet,²⁸ S.S. Ryu,⁵² M.E. Sadler,¹ N. Saito,^{38,39} T. Sakaguchi,^{8,50} M. Sakai,³² S. Sakai,⁴⁸ V. Samsonov,³⁷ L. Sanfratello,³³ R. Santo,³⁰ H.D. Sato,^{24,38} S. Sato,^{5,48} S. Sawada,²⁰ Y. Schutz,⁴⁵ V. Semenov,¹⁵ R. Seto,⁶ M.R. Shaw,^{1,27} T.K. Shea,⁵ T.-A. Shibata,^{47,38} K. Shigaki,^{14,20} T. Shiina,²⁷ C.L. Silva,⁴¹ D. Silvermyr,^{27,29} K.S. Sim,²² C.P. Singh,³ V. Singh,³ M. Sivertz,⁵ A. Soldatov,¹⁵ R.A. Soltz,²⁶ W.E. Sondheim,²⁷ S.P. Sorensen,⁴⁶ I.V. Sourikova,⁵ F. Staley,¹⁰ P.W. Stankus,³⁵ E. Stenlund,²⁹ M. Stepanov,³⁴ A. Ster,²¹ S.P. Stoll,⁵ T. Sugitate,¹⁴ J.P. Sullivan,²⁷ E.M. Takagui,⁴¹ A. Takiuchi,^{38,39} M. Tamai,⁵⁰ K.H. Tanaka,²⁰ Y. Tanaka,³² K. Tanida,³⁸ M.J. Tannenbaum,⁵ P. Tarján,¹¹ J.D. Tepe,^{1,27} T.L. Thomas,³³ J. Tojo,^{24,38} H. Torii,^{24,38} R.S. Towell,¹ I. Tserruya,⁵¹ H. Tsuruoka,⁴⁸ S.K. Tuli,³ H. Tydesjö,²⁹ N. Tyurin,¹⁵ H.W. van Hecke,²⁷ J. Velkovska,^{5,44} M. Velkovsky,⁴⁴ L. Villatte,⁴⁶ A.A. Vinogradov,²³ M.A. Volkov,²³ E. Vznuzdaev,³⁷ X.R. Wang,¹³ Y. Watanabe,^{38,39} S.N. White,⁵ F.K. Wohn,¹⁶ C.L. Woody,⁵ W. Xie,⁶ Y. Yang,⁷ A. Yanovich,¹⁵ S. Yokkaichi,^{38,39} G.R. Young,³⁵ I.E. Yushmanov,²³ W.A. Zajc,^{9,†} C. Zhang,⁹ S. Zhou,^{7,51} and L. Zolin¹⁷

(PHENIX Collaboration)

¹Abilene Christian University, Abilene, TX 79699, USA

²Institute of Physics, Academia Sinica, Taipei 11529, Taiwan

³Department of Physics, Banaras Hindu University, Varanasi 221005, India

⁴Bhabha Atomic Research Centre, Bombay 400 085, India

⁵Brookhaven National Laboratory, Upton, NY 11973-5000, USA
⁶University of California - Riverside, Riverside, CA 92521, USA
⁷China Institute of Atomic Energy (CIAE), Beijing, People's Republic of China
⁸Center for Nuclear Study, Graduate School of Science, University of Tokyo, 7-3-1 Hongo, Bunkyo, Tokyo 113-0033, Japan
⁹Columbia University, New York, NY 10027 and Nevis Laboratories, Irvington, NY 10533, USA
¹⁰Dapnia, CEA Saclay, F-91191, Gif-sur-Yvette, France
¹¹Debrecen University, H-4010 Debrecen, Egyetem tér 1, Hungary
¹²Florida State University, Tallahassee, FL 32306, USA
¹³Georgia State University, Atlanta, GA 30303, USA
¹⁴Hiroshima University, Kagamiyama, Higashi-Hiroshima 739-8526, Japan
¹⁵Institute for High Energy Physics (IHEP), Protvino, Russia
¹⁶Iowa State University, Ames, IA 50011, USA
¹⁷Joint Institute for Nuclear Research, 141980 Dubna, Moscow Region, Russia
¹⁸KAERI, Cyclotron Application Laboratory, Seoul, South Korea
¹⁹Kangnung National University, Kangnung 210-702, South Korea
²⁰KEK, High Energy Accelerator Research Organization, Tsukuba-shi, Ibaraki-ken 305-0801, Japan
²¹KFKI Research Institute for Particle and Nuclear Physics (RMKI), H-1525 Budapest 114, POBox 49, Hungary
²²Korea University, Seoul, 136-701, Korea
²³Russian Research Center "Kurchatov Institute", Moscow, Russia
²⁴Kyoto University, Kyoto 606, Japan
²⁵Laboratoire Leprince-Ringuet, Ecole Polytechnique, CNRS-IN2P3, Route de Saclay, F-91128, Palaiseau, France
²⁶Lawrence Livermore National Laboratory, Livermore, CA 94550, USA
²⁷Los Alamos National Laboratory, Los Alamos, NM 87545, USA
²⁸LPC, Université Blaise Pascal, CNRS-IN2P3, Clermont-Fd, 63177 Aubiere Cedex, France
²⁹Department of Physics, Lund University, Box 118, SE-221 00 Lund, Sweden
³⁰Institut für Kernphysik, University of Muenster, D-48149 Muenster, Germany
³¹Myongji University, Yongin, Kyonggido 449-728, Korea
³²Nagasaki Institute of Applied Science, Nagasaki-shi, Nagasaki 851-0193, Japan
³³University of New Mexico, Albuquerque, NM, USA
³⁴New Mexico State University, Las Cruces, NM 88003, USA
³⁵Oak Ridge National Laboratory, Oak Ridge, TN 37831, USA
³⁶IPN-Orsay, Université Paris Sud, CNRS-IN2P3, BP1, F-91406, Orsay, France
³⁷PNPI, Petersburg Nuclear Physics Institute, Gatchina, Russia
³⁸RIKEN (The Institute of Physical and Chemical Research), Wako, Saitama 351-0198, JAPAN
³⁹RIKEN BNL Research Center, Brookhaven National Laboratory, Upton, NY 11973-5000, USA
⁴⁰St. Petersburg State Technical University, St. Petersburg, Russia
⁴¹Universidade de São Paulo, Instituto de Física, Caixa Postal 66318, São Paulo CEP05315-970, Brazil
⁴²System Electronics Laboratory, Seoul National University, Seoul, South Korea
⁴³Chemistry Department, Stony Brook University, SUNY, Stony Brook, NY 11794-3400, USA
⁴⁴Department of Physics and Astronomy, Stony Brook University, SUNY, Stony Brook, NY 11794, USA
⁴⁵SUBATECH (Ecole des Mines de Nantes, CNRS-IN2P3, Université de Nantes) BP 20722 - 44307, Nantes, France
⁴⁶University of Tennessee, Knoxville, TN 37996, USA
⁴⁷Department of Physics, Tokyo Institute of Technology, Tokyo, 152-8551, Japan
⁴⁸Institute of Physics, University of Tsukuba, Tsukuba, Ibaraki 305, Japan
⁴⁹Vanderbilt University, Nashville, TN 37235, USA
⁵⁰Waseda University, Advanced Research Institute for Science and Engineering, 17 Kikui-cho, Shinjuku-ku, Tokyo 162-0044, Japan
⁵¹Weizmann Institute, Rehovot 76100, Israel
⁵²Yonsei University, IPAP, Seoul 120-749, Korea

(Dated: February 9, 2020)

Event-by-event fluctuations of the average transverse momentum of produced particles near mid-rapidity have been measured by the PHENIX Collaboration in $\sqrt{s_{NN}} = 200$ GeV Au+Au and p+p collisions at the Relativistic Heavy Ion Collider. The fluctuations are observed to be in excess of the expectation for statistically independent particle emission for all centralities. The excess fluctuations exhibit a dependence on both the centrality of the collision and on the p_T window over which the average is calculated. This behavior is consistent with a scenario whereby the predominant contribution to the excess is due to jets where the high p_T hadron production is suppressed in the most central collisions.

PACS numbers: 25.75.Dw

The measurement of fluctuations in the event-by-event average transverse momentum of produced particles in

relativistic heavy ion collisions has been proposed as a probe of phase instabilities near the QCD phase transition [1, 2, 3], which could result in classes of events with different properties, such as the effective temperature of the collision. Fluctuation measurements could also provide information about the onset of thermalization in the system [4]. The resulting phenomena can be observed by measuring deviations of the event-by-event average p_T , referred to here as M_{p_T} , of produced charged particles from the expectation for statistically independent particle emission [5, 6] after subtracting contributions from fluctuations arising from physical processes such as elliptic flow and jet production.

Several M_{p_T} fluctuation measurements have been reported in heavy ion collisions [7, 8, 9, 10], including a study by PHENIX [9] in $\sqrt{s_{NN}} = 130$ GeV Au+Au collisions which set limits on the magnitude of non-random fluctuations in M_{p_T} . Recently, STAR has reported fluctuations in excess of the random expectation, within the PHENIX limits, at the same collision energy [10]. For these first results from $\sqrt{s_{NN}} = 200$ GeV Au+Au and p+p collisions reported here, upgrades of the PHENIX central arm spectrometers [11] have expanded the azimuthal acceptance from 58.5° to 180.0° within the pseudorapidity range of $|\eta| < 0.35$. Pad chamber and calorimeter detectors have also been installed for improved background rejection. Coupled with an increase in the number of analyzed events, the sensitivity of the PHENIX spectrometer to the observation of fluctuations in M_{p_T} due to event-by-event fluctuations in the effective temperature [9, 12] has improved by greater than a factor of two.

Minimum bias events triggered by a coincidence between the Zero Degree Calorimeters (ZDC) and the Beam-Beam Counters (BBC) with a requirement that the collision vertex, which is measured with an r.m.s. resolution of less than 6 mm in central collisions and 8 mm in the most peripheral collisions, be within 5 cm of the nominal origin are used in this analysis. Event centrality for Au+Au collisions, which is defined using correlations in the BBC and ZDC analog response [13], is divided into several classes, each containing over 200,000 analyzed events. These classes are associated to the estimated average number of participants in the collision, $\langle N_{part} \rangle$, which is derived using a Glauber model Monte Carlo calculation with the BBC and ZDC detector response taken into account [14].

Charged particle momenta are reconstructed in the PHENIX central arm spectrometers with a drift chamber and a radially adjacent pixel pad chamber. Non-vertex track background rejection is provided by pixel pad chambers and calorimeters located further outward radially from the collision vertex [15]. The momentum resolution is $\frac{\delta p}{p} \simeq 0.7\% \oplus 1.0\% \times p$ (GeV/c).

M_{p_T} is calculated for each event, which contains a number of reconstructed tracks within a specified p_T

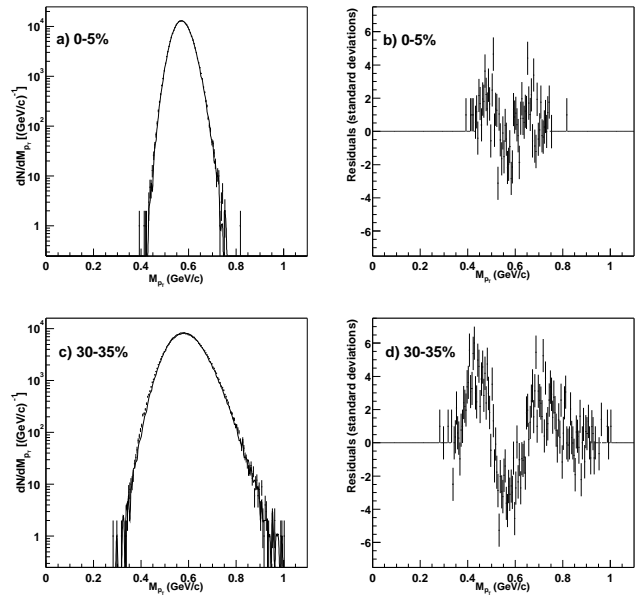


FIG. 1: Comparisons between the data and mixed event M_{p_T} distributions for the representative 0-5% and 30-35% centrality classes. Plots a) and c) show direct comparisons of the data (points) and normalized mixed event (solid line) M_{p_T} distributions. Plots b) and d) show the residuals between the data and mixed events in units of standard deviations of the data points from the mixed event points.

range, N_{tracks} . The p_T range is always given a lower bound of 200 MeV/c and a varying upper bound, p_T^{max} , from 500 MeV/c to 2.0 GeV/c. There is a minimum N_{tracks} cut of 3 in both Au+Au events (removing 0%, 4.6%, and 29% of events in the 0-50%, 50-60%, and 60-70% centrality bins, respectively, when $p_T^{max} = 2.0$ GeV/c) and p+p events (removing 59% of the events).

There are several measures by which the magnitude of non-random fluctuations can be quantified, namely ϕ_{p_T} [16, 17], $\nu_{dynamic}$ [18], and F_{p_T} [9]. The calculation of F_{p_T} is based upon the magnitude of the fluctuation, ω_{p_T} , defined as

$$\omega_{p_T} = \frac{(\langle M_{p_T}^2 \rangle - \langle M_{p_T} \rangle^2)^{1/2}}{\langle M_{p_T} \rangle} = \frac{\sigma_{M_{p_T}}}{\langle M_{p_T} \rangle}. \quad (1)$$

F_{p_T} is defined as the fractional deviation of ω_{p_T} from a baseline estimate defined using mixed events [9],

$$F_{p_T} = \frac{(\omega_{(p_T, data)} - \omega_{(p_T, mixed)})}{\omega_{(p_T, mixed)}}. \quad (2)$$

Mixed event M_{p_T} distributions are validated by comparisons to a calculation of M_{p_T} assuming statistically independent particle emission using parameters extracted from the inclusive p_T distributions of the data [19]. For the 0-5% centrality class, which suffers the most from tracking inefficiency, the effects of two-track resolution,

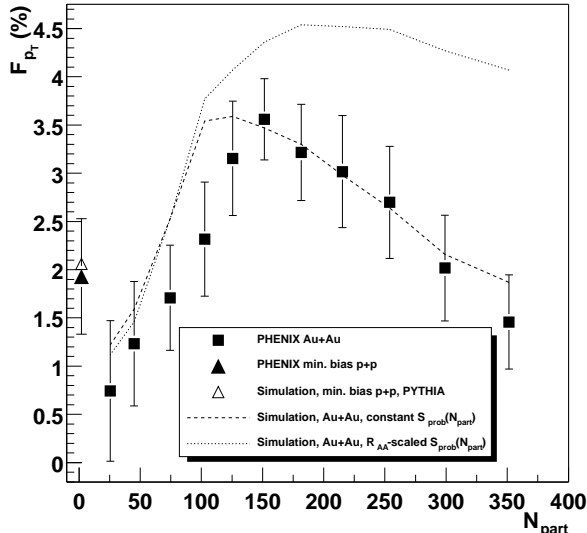


FIG. 2: F_{p_T} (in percent, $0.2 \text{ GeV}/c < p_T < 2.0 \text{ GeV}/c$) as a function of centrality, which is expressed in terms of the number of participants in the collision, N_{part} . The solid squares represent the Au+Au data. The solid triangle represents the minimum bias p+p data point. The open triangle is the result from an analysis of PYTHIA minimum bias p+p events within the PHENIX acceptance. The error bars include statistical and systematic errors and are dominated by the latter. The curves are the results of a Monte Carlo simulation with hard processes modelled using PYTHIA with a constant (dotted curve) and R_{AA} -scaled (dashed curve) hard scattering probability factor, and include the estimated contribution due to elliptic flow.

and background contributions, the mixed event M_{p_T} distribution yields a value of $F_{p_T} = 0.04\%$ with respect to the calculation. The results of this comparison are included in the estimates of the systematic errors.

Comparisons of the data and mixed event M_{p_T} distributions for the 0-5% and 30-35% centrality classes are shown in Fig. 1. Any excess fluctuations are small and are difficult to distinguish by eye in a direct overlay of the M_{p_T} distributions. Therefore, the comparison is also shown as residuals between the data and mixed event distributions in units of standard deviations of the data points from the mixed event points. The double-peaked shape in the residual distributions is an artifact of the fact that the mixed event distributions, which always have a smaller standard deviation in M_{p_T} than the data, are normalized to minimize the total χ^2 of the residual distribution.

Figure 2 shows the magnitude of F_{p_T} , expressed in percent, as a function of centrality for Au+Au collisions with $p_T^{\max} = 2.0 \text{ GeV}/c$. The error bars are dominated by time-dependent systematic effects during the data taking period due to detector variations, which are minimized

using strict time-dependent cuts on the mean and standard deviations of the inclusive p_T and N_{tracks} distributions. The systematic errors are determined by dividing the entire dataset into ten separate subsets for each centrality class and extracting the standard deviation of the F_{p_T} values calculated for each subset. From Fig. 2, a significant non-random fluctuation is seen that appears to peak in mid-central collisions. However, the magnitude of the observed fluctuations are within previously published limits [9]. In addition, the value of F_{p_T} for the most peripheral Au+Au collisions is consistent with, albeit slightly below, the value measured by the same PHENIX apparatus in minimum bias $\sqrt{s_{NN}} = 200 \text{ GeV}$ p+p collisions. If the magnitude of F_{p_T} is entirely due to fluctuations in the effective temperature of the system [12], this measurement corresponds to a fluctuation of $\sigma_T / \langle T \rangle = 1.8\%$ at 0-5% centrality and 3.7% at 20-25% centrality.

To further understand the source of the non-random fluctuations, F_{p_T} is measured over a varying p_T range for which M_{p_T} is calculated, $0.2 \text{ GeV}/c < p_T < p_T^{\max}$. Figure 3 shows F_{p_T} plotted as a function of p_T^{\max} for the 20-25% centrality class. A trend of increasing F_{p_T} for increasing p_T^{\max} is observed for this and all other centrality classes. The majority of the contribution to F_{p_T} appears to be due to correlations of particles with $p_T > 0.8 \text{ GeV}/c$, where F_{p_T} increases disproportionately to the small increase of N_{tracks} in this region.

The behavior of F_{p_T} as a function of centrality and p_T is similar to trends seen in measurements of elliptic flow [20]. The contribution of elliptic flow to the magnitude of F_{p_T} is investigated using a Monte Carlo simulation. Each simulated event is assigned N_{tracks} particles by sampling a Gaussian fit to the data N_{tracks} distribution and assigned a random reaction plane azimuthal angle, Φ , between 0 and 2π . Each particle within an event is assigned a p_T value by sampling a double exponential fit in p_T to the data over $0.2 \text{ GeV}/c < p_T < 2.0 \text{ GeV}/c$. Each particle in an event is also assigned an azimuthal angle, ϕ , by sampling the function $\frac{dN}{d(\phi - \Phi)} = 1 + 2v_2 \cos(2(\phi - \Phi))$. The values of the v_2 parameter are linearly parameterized as a function of p_T and centrality using PHENIX measurements of inclusive charged hadrons [20]. A particle is included in the calculation of M_{p_T} only if its azimuthal angle is within the PHENIX azimuthal acceptance. This simulation estimates that the contribution of elliptic flow to F_{p_T} is largely cancelled out by the symmetry of the PHENIX acceptance, and is negligible for central collisions. The elliptic flow contribution to the value of F_{p_T} is estimated to be less than 0.1% for $N_{\text{part}} > 150$, increasing to about 0.6% for $N_{\text{part}} < 100$. Note that F_{p_T} measured for minimum bias p+p collisions, where flow is not expected to contribute, is non-zero ($1.9 \pm 0.6\%$), implying that a non-flow contribution may also be present in peripheral Au+Au collisions.

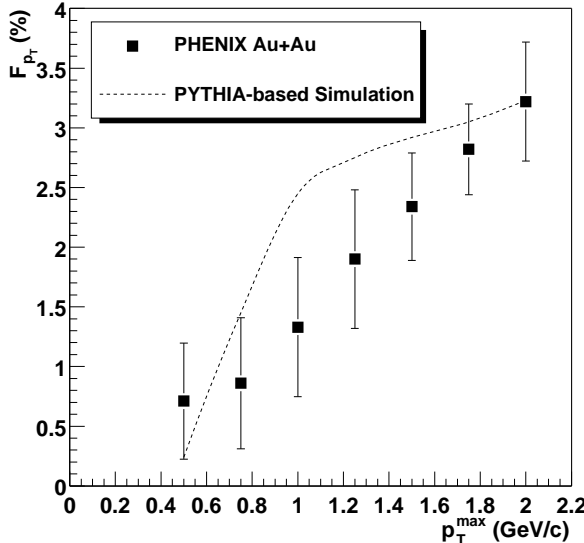


FIG. 3: F_{p_T} (in percent) of non-random fluctuations as a function of the p_T range over which M_{p_T} is calculated, $0.2 \text{ GeV}/c < p_T < p_T^{\max}$, for the 20-25% centrality class ($N_{part}=181.6$). The curve is the result of a Monte Carlo simulation with hard processes modelled using PYTHIA. The error bars include statistical and systematic errors and are dominated by the latter. The contribution of elliptic flow is estimated to be negligible at this centrality.

Figure 3 illustrates that a large contribution to the observed non-random fluctuations is due to the correlation of high p_T particles, such as might be expected from correlations due to jet production [21]. In order to investigate the contribution due to jets, a Monte Carlo simulation is again consulted. The same method previously described is applied, only the p_T assignment is made by sampling an exponential function in m_T , which describes the p_T spectra reasonably well for $p_T < 2.0 \text{ GeV}/c$ [22]. The parameters of this function, $f(p_T)$, are determined for each centrality class by fitting to the data p_T distribution, $d(p_T)$. For a given value of p_T , a probability that a hard scattering process occurs is defined as $P(p_T) = 1 - (f(p_T)/d(p_T))$. Since the nuclear medium can affect $P(p_T)$ in more central collisions [22], the $P(p_T)$ distribution extracted from the most peripheral (60-70% centrality) collisions is applied to all centrality classes. If an assigned p_T value tests positive against $P(p_T)$, then a hard process is assumed to have occurred, and a single $\sqrt{s_{NN}} = 200 \text{ GeV}$ p+p hard scattering process event generated by the PYTHIA event generator [23] is embedded into the event being constructed. After N_{tracks} particles have been generated, M_{p_T} is calculated. The addition of the PYTHIA events affects the mean and standard deviation of the inclusive p_T spectra by less than 0.1%. In order to validate the use of PYTHIA events, the value

of F_{p_T} has been extracted from 100,000 PYTHIA minimum bias p+p events, yielding $F_{p_T}=2.06\%$ within the PHENIX acceptance, which is consistent with the measured value of $F_{p_T} = 1.9 \pm 0.6\%$.

Simulations of the centrality dependence of the fluctuations are allowed a single varying parameter, $S_{prob}(N_{part})$, which is a scaling factor by which $P(p_T)$ is multiplied for a given centrality. The simulation is studied using two methods: 1) with $S_{prob}(N_{part})$ fixed for all centrality classes, and 2) with $S_{prob}(N_{part})$ scaled for each centrality class by the PHENIX measurement of the suppression of high p_T charged particles, which is characterized by the nuclear modification factor, R_{AA} , integrated over $p_T > 4.5 \text{ GeV}/c$ [24]. The p_T value at which R_{AA} is extracted has little effect on the simulation results, which change by less than 0.2% for 0-5% centrality if the R_{AA} measurement at $p_T = 2.0 \text{ GeV}/c$ is used instead. The latter method is intended to model the effect of the suppression of jets due to energy loss in the nuclear medium [22] on the fluctuation signal. The initial value of $S_{prob}(N_{part})$ for both methods is normalized so that the F_{p_T} quantity from the R_{AA} -scaled simulation matches that of the data near the peak for the 20-25% centrality class. The results of the simulation as a function of p_T^{\max} , with $S_{prob}(N_{part})$ scaled by R_{AA} , are shown in Fig. 3 for the 20-25% centrality class, represented by the dashed curve. The trend of increasing F_{p_T} with increasing p_T^{\max} observed in the data is reproduced by the simulation reasonably well.

The results of the two hard scattering simulation methods are shown in Fig. 2 as a function of centrality. The model curves include the small contribution estimated from the elliptic flow simulation. The dotted curve is the result with $S_{prob}(N_{part})$ fixed for all centralities. The dashed curve is the result with $S_{prob}(N_{part})$ scaled by R_{AA} as a function of centrality. Within this simulation, the decrease of F_{p_T} for the more peripheral events is explained as a decrease in the signal strength due to the small and decreasing value of N_{tracks} . If $S_{prob}(N_{part})$ remains constant, the expectation is that the value of F_{p_T} decreases only slightly when going from mid-central to central collisions, in contradiction with the decrease seen in the data over this centrality range. When $S_{prob}(N_{part})$ is scaled by R_{AA} as a function of centrality, the trend in the simulation of decreasing F_{p_T} with increasing centrality is consistent with the data.

To summarize, the PHENIX experiment has observed a positive non-random fluctuation signal in event-by-event average transverse momentum, measured as a function of centrality and p_T in $\sqrt{s_{NN}} = 200 \text{ GeV}$ Au+Au and p+p collisions. The increase of F_{p_T} with increasing p_T implies that the majority of the fluctuations are due to correlated high p_T particles. A Monte Carlo simulation that includes elliptic flow and a PYTHIA-based hard scattering description can consistently describe the data in the case where a modelling of jet suppression via the

scaling of a hard scattering probability by the measured value of R_{AA} as a function of centrality is invoked.

We thank the staff of the Collider-Accelerator and Physics Departments at BNL for their vital contributions. We acknowledge support from the Department of Energy and NSF (U.S.A.), MEXT and JSPS (Japan), CNPq and FAPESP (Brazil), NSFC (China), CNRS-IN2P3 and CEA (France), BMBF, DAAD, and AvH (Germany), OTKA (Hungary), DAE and DST (India), ISF (Israel), KRF and CHEP (Korea), RMIST, RAS, and RMAE, (Russia), VR and KAW (Sweden), U.S. CRDF for the FSU, US-Hungarian NSF-OTKA-MTA, and US-Israel BSF.

Rev. **C66**, 024901 (2002).

- [10] STAR Collaboration, preprint nucl-ex/0308033, to be published.
- [11] PHENIX Collaboration, K. Adcox *et al.*, Nucl. Instrum. Methods **A499**, 235 (2003).
- [12] R. Korus and S. Mrówczyński, Phys. Rev. **C64**, 054908 (2001).
- [13] PHENIX Collaboration, K. Adcox *et al.*, Phys. Rev. Lett. **86**, 3500 (2001).
- [14] PHENIX Collaboration, preprint nucl-ex/0307022, to be published.
- [15] J. T. Mitchell *et al.*, Nucl. Instrum. Methods **A482**, 491 (2002).
- [16] M. Gaździcki and S. Mrówczyński, Z. Phys. **C54**, 127 (1992).
- [17] S. Mrówczyński, Phys. Lett. **B439**, 6 (1998).
- [18] C. Pruneau *et al.*, Phys. Rev. **C66**, 044904 (2002).
- [19] M. J. Tannenbaum, Phys. Lett. **B498**, 29 (2001).
- [20] PHENIX Collaboration, S. S. Adler *et al.*, preprint nucl-ex/0305013, to be published; PHENIX Collaboration, K. Adcox *et al.*, Phys. Rev. Lett. **89**, 212301 (2002); STAR Collaboration, C. Adler *et al.* Phys. Rev. **C66**, 034904 (2002).
- [21] Q. Liu and T. Trainor, Phys. Lett. **B567**, 184 (2003).
- [22] X. N. Wang, Phys. Rev. **C58**, 2321 (1998).
- [23] T. Sjöstrand, Computer Physics Commun. **82**, 74 (1994). Version 5.720 with MSEL=1 for embedded hard scattering events and MSEL=2 for min. bias p+p events, CKIN(3)=0.0, MSTP(32)=4, and MSTP(33)=1.
- [24] PHENIX Collaboration, preprint nucl-ex/0308006, to be published.

* Deceased

† PHENIX Spokesperson:zajc@nevis.columbia.edu

- [1] H. Heiselberg, Phys. Repts. **351**, 161 (2001).
- [2] M. Stephanov *et al.*, Phys. Rev. Lett. **81**, 4816 (1998).
- [3] M. Stephanov *et al.*, Phys. Rev. **D60**, 114028 (1999).
- [4] S. Gavin, nucl-th/0308067, to be published.
- [5] L. Stodolsky, Phys. Rev. Lett. **75**, 1044 (1995).
- [6] E. Shuryak, Phys. Lett. **B423**, 9 (1998).
- [7] NA49 Collaboration, H. Appelshäuser *et al.*, Phys. Lett. **B459**, 679 (1999).
- [8] CERES Collaboration, D. Adamová *et al.*, Nucl. Phys. **A727**, 97 (2003).
- [9] PHENIX Collaboration, K. Adcox *et al.*, Phys.